Journal of Photochemistry and Photobiology A: Chemistry 211 (2010) 47–58

Contents lists available at ScienceDirect

Journal of Photochemistry and Photobiology A: Chemistry

journal homepage: www.elsevier.com/locate/jphotochem

Photoinduced processes of 3-substituted 6-fluoro-1,4-dihydro-4-oxoquinoline derivatives: A theoretical and spectroscopic study

Ján Rimarčík[a], Vladimír Lukeš[a,*], Erik Klein[a], Anne-Marie Kelterer[b], Viktor Milata[c], Zuzana Vrecková[a], Vlasta Brezová[a]

[a] Institute of Physical Chemistry and Chemical Physics, Faculty of Chemical and Food Technology, Slovak University of Technology in Bratislava, Radlinského 9, SK-812 37 Bratislava, Slovak Republic
[b] Institute of Physical and Theoretical Chemistry, Graz University of Technology, Technikerstrasse 4/I, A-8010 Graz, Austria
[c] Institute of Organic Chemistry, Catalysis and Petrochemistry, Faculty of Chemical and Food Technology, Slovak University of Technology in Bratislava, Radlinského 9, SK-812 37 Bratislava, Slovak Republic

ARTICLE INFO

Article history:
Received 7 September 2009
Received in revised form 26 January 2010
Accepted 8 February 2010
Available online 16 February 2010

Keywords:
Fluoroquinolones
Photosensitive drugs
Molecular oxygen
ROS
TD-DFT
RI-CC2
Ionization potential
Electron affinity
EPR

ABSTRACT

Presented computational study of 3-substituted 6-fluoro-1,4-dihydro-4-oxoquinoline derivatives confirmed the existence of two tautomeric (oxo- and hydroxy-) forms of these molecules originating from the presence of 4-oxo substitution on quinoline skeleton. The computed singlet excitation energies at the time-dependent density functional theory (DFT) level and the simulated absorption spectra are in accordance with the experimental UV/vis spectra measured in aprotic solvents (1,4-dioxane, acetonitrile, dimethylsulfoxide). Measured spectra indicate the solvent capability to affect the ratio of tautomeric forms in the solution. Reaction pathways of $O_2^{\bullet-}$ and singlet oxygen ($^1\Delta_g$) formation and the energetics of these processes were studied using TD-DFT including the solvent effect in terms of polarizable continuum model. EPR spectroscopy confirmed that photoinduced reactions of 3-substituted 6-fluoro-1,4-dihydro-4-oxoquinoline derivatives with molecular oxygen lead to $O_2^{\bullet-}$ and singlet oxygen ($^1\Delta_g$) formation.

© 2010 Elsevier B.V. All rights reserved.

1. Introduction

4-Oxoquinolines represent a group of heterocyclic compounds with multispectral biological activity, mainly antibacterial (inhibitors of DNA gyrase, topoisomerase IV), multispectral antitumor, coccidiostatic and even antiviral activity [1–4]. Nowadays, fluoro-substituted 4-oxoquinoline-3-carboxylic acids (e.g. norfloxacin, ciprofloxacin, ofloxacin, sparfloxacin, enoxacin) are applied in the medical care as broad-spectrum antibiotics [2]. Previously it was found that upon UVA irradiation (315–400 nm) fluoroquinolones induce photosensitized reactions with phototoxic and photoallergic responses [5–9]. Consequently, a great attention was focused on the investigation of their photoinduced processes [10–23]. The phototoxicity of an individual drug can be controlled by different mechanisms, and its biologic effects (phototoxic, photomutagenic, photocancerogenic) vary depending on cell type, drug uptake, tissue, cellular and subcellular localization [24–26]. According to the literature data the phototoxic reactions have been classified into four groups [24,25]: (i) the generation of toxic photoproducts; (ii) direct interaction with DNA; (iii) Type I photooxidation reactions resulting in the formation of Reactive Oxygen Species (ROS), e.g. $O_2^{\bullet-}$, $HOO^{\bullet}$, H_2O_2; (iv) Type II photooxidation process generating singlet oxygen ($^1O_2$). The investigation of structure–phototoxicity relationship revealed that the phototoxic impact of fluoroquinolone derivatives is influenced not only by the substituent at C8 atom, but also by that at N1 [12,13,27–29] (Fig. 1). The photoexcitation of 6-monofluoroquinolones in aqueous solutions resulted in the replacement of fluorine atom by hydroxyl

Abbreviations: ACN, acetonitrile; AEA, adiabatic electron affinity; AIP, adiabatic ionization potential; DMPO, 5,5-dimethyl-1-pyrroline *N*-oxide; DFT, density functional theory; DIOX, 1,4-dioxane; DMSO, dimethylsulfoxide; EPR, electron paramagnetic resonance; Hfcc, hyperfine coupling constants; HOMO, highest occupied molecular orbital; HWHH, half-width at half-height; IEF-PCM, integral equation formalism polarizable continuum model; LUMO, lowest unoccupied molecular orbital; PCM, polarizable continuum model; QE, quantum efficiency; RI-CC2, Coupled Cluster Singles and Doubles with Resolution of Identity; ROS, reactive oxygen species; SW, magnetic field sweep width; TD-DFT, time-dependent DFT; TEMPOL, 4-hydroxy-2,2,6,6-tetramethylpiperidine *N*-oxyl; TMP, 4-hydroxy-2,2,6,6-tetramethylpiperidine; UV/vis, ultraviolet/visible; UVA, ultraviolet, A region; VEA, vertical electron affinity; VIP, vertical ionization potential; ZPE, zero point energy.

* Corresponding author. Tel.: +421 2 5932 57 41; fax: +421 2 5292 6032.
E-mail address: vladimir.lukes@stuba.sk (V. Lukeš).

1010-6030/$ – see front matter © 2010 Elsevier B.V. All rights reserved.
doi:10.1016/j.jphotochem.2010.02.001

group *via* various reaction pathways [10,13–16,19,30,31]. On the other hand, defluorination of 6,8-difluoroquinolones *via* unimolecular fragmentation was proposed [11,12]. Possible photoreactivity channels of fluoroquinolone drugs are also discussed in the literature [9,24,32,33]. The photoinstability of fluoroquinolones upon UVA irradiation often causes the loss of their antimicrobial activity, but photoinstability does not necessarily mean phototoxic effect of drug *in vivo* [24,33].

UVA exposure of rat liver cells in the presence of lomefloxacin resulted in DNA damage related to the formation of singlet oxygen and hydroxyl radicals, considering both Type I and Type II photooxidation processes [24,33]. Previously, Umezawa et al. confirmed the photoinduced generation of superoxide radical anion ($O_2^{\bullet-}$) and $^1O_2$ upon irradiation of fluoroquinolone antibiotics, i.e. lomefloxacin, enoxacin, ofloxacin and ciprofloxacin. Investigated drugs caused photoinduced DNA strand-breaking dependent on the binding affinity of fluoroquinolone to DNA [20]. The ability of fluoroquinolone drugs to produce $O_2^{\bullet-}$ upon irradiation ($\lambda > 300$ nm) in dimethylsulfoxide (DMSO) was monitored by EPR spin trapping technique using 5,5-dimethyl-1-pyrroline *N*-oxide (DMPO) as the spin trap, and the quantum yield of $^1O_2$ generation was evaluated by luminescence detection at 1270 nm [17,18,34,35]. However, obtained results did not explain a high phototoxicity of fluoroquinolone derivatives with halogen atom at C8 position [32]. Consequently, the generation of reactive carbene structure after photoinduced loss of fluorine atom at C8 was assumed [17].

Theoretical quantum chemical studies of π-conjugated systems can provide a fundamental understanding and considerable contribution to the design of novel molecules with improved chemical or biological properties. Musa and Eriksson [36] used density functional theory (DFT) approach to study the photodegradation mechanism of diclofenac, the common non-steroid anti-inflammatory drug. Photoreactivity of diclofenac and products of its photodegradation were studied at the B3LYP/6-31G(d,p) level of theory. UV/vis spectra obtained using TD-DFT were in line with experimental ones, confirming the method is suitable for theoretical study of similar molecules. Theoretical studies [37,38] employed semiempirical, *ab initio* and DFT methods, especially for the optimal geometries and electronic structures of organic molecules. Among them, the DFT approach [39] and its time-dependent (TD) extension [40,41] for the excited states can be successfully applied for the investigation of optical and electronic properties of various molecules.

Our study is focused on the theoretical and experimental investigations of effect of substituent at C3 atom on the electronic spectra of newly synthesized 3-R-6-fluoro-1,4-dihydro-4-oxoquinoline derivatives (R = H, $COOCH_2CH_3$, $COOCH_3$, CN, $COCH_3$, Fig. 1). The ability of these fluoroquinolone derivatives to produce ROS ($O_2^{\bullet-}$ and $^1O_2$) upon UVA irradiation in the presence of molecular oxygen was investigated by means of *in situ* EPR spectroscopy. Theoretical investigations were performed at the DFT level of theory. For the obtained optimal DFT geometries, the vertical ionization potentials and electron affinities were calculated. Vertical excited state energies were obtained using TD-DFT method. The computational results were used to interpret experimental UV/vis spectra measured in aprotic solvents. The physical origin of the lowest electronic transition was explained using molecular orbital analysis. Study of energetics of the processes of ROS formation also represents one of the crucial aims of this work.

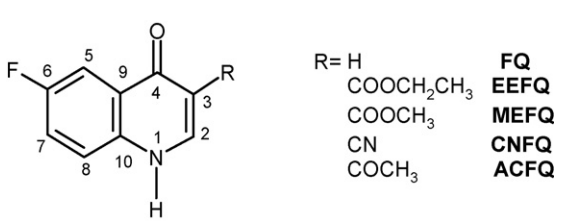

Fig. 1. Structure, atom numbering and denotation of the investigated fluoroquinolone molecules.

2. Calculation and experimental details

2.1. Calculation methods

The electronic ground state geometries of the studied molecules were optimized at the DFT level of theory employing Becke's three parameter hybrid functional using the Lee, Yang and Parr correlation functional for Gaussian 03 (B3LYP) [42]. For solution-phase calculations the integral equation formalism polarizable continuum model (IEF-PCM) approach was used [43,44]. In general, the polarizable continuum model offers good accuracy and reliability [45–47]. The method has been widely adopted in recent years, especially in the description of the thermodynamic characteristics of solvation [48–51]. It also reduces the computational effort in the study of solvent effects. The calculations were performed using the 6-31+G(d) basis set [52,53] (the energy cut-off of 4×10^{-3} kJ mol^{-1} and the final root mean square energy gradient below 0.04 kJ mol^{-1} Å^{-1}). The obtained optimal structures were confirmed by normal mode analysis (no imaginary frequencies for all optimal geometries). The numerical integration of the DFT functional was performed using default fine integration grid.

On the basis of optimized geometries, the vertical transition energies and oscillator strengths between the initial and final states were computed by TD-DFT method in the 6-31+G(d) basis set. To ensure that the chosen basis set is sufficiently large, for the pristine molecule **FQ**, the calculation of the vertical transition energies and oscillator strengths was performed in 6-311++G(2df,2pd) [54], aug-cc-pVDZ, and aug-cc-pVTZ basis sets [55].

We should note that TD-DFT is known to incorrectly represent excited states when the electronic excitation corresponds to the charge transfer between the two rings [56,57]. However, the investigated 3-substituted 1,4-dihydro-6-fluoro-4-oxoquinoline derivatives are substituted at benzene moiety only with fluorogroup at C6, and no electron donor is present. Additionally, the photochemical experiments were performed in organic solvents (DMSO and ACN), in which the formation of the intramolecular charge transfer is not preferred, also when its formation is possible. Consequently, on the basis of performed experiments and according the literature data related to other fluoroquinolone drugs [58–60] it is plausible to assume that the formation of zwitterion structure including benzene and 4-pyridone moieties, as well as intramolecular charge transfer between them is not characteristic of studied 3-substituted 6-fluoro-1,4-dihydro-4-oxoquinoline derivatives. Consequently, the theoretical calculations of these molecules using TD-B3LYP is adequate for the interpretation of electronic spectra measured in aprotic organic solvents in our study. Additionally, TD-B3LYP method for the calculation of the excited states of quinolones was applied recently in the study of 1-ethyl-6,8-difluoro-7-(3-methylpiperazin-1-yl)-3-quinolone-2-carboxylic acid [11].

Besides, we have also calculated TD-PBE0/6-31+G(d) vertical excitation energies and the oscillator strengths for the studied molecules in ACN. PBE0 [61] functional was chosen, because it was reported that this functional is able to provide vertical excitation energies [62] of various small and medium-size molecules in good agreement with experimental data and more computationally demanding methods. For the sake of comparison, *ab initio* single point benchmark calculations were also performed using the RI-CC2 (Coupled Cluster Singles and Doubles with Resolution of

Identity) method [63]. All TD-DFT calculations were done using the Gaussian 03 [64] program package. The benchmark RI-CC2 calculations were performed using Turbomole 5.10 program package [65,66].

2.2. Chemicals and reagents

The 3-R-6-fluoro-1,4-dihydro-4-oxoquinoline derivatives, R = H (**FQ**), $COOCH_2CH_3$ (**EEFQ**), $COOCH_3$ (**MEFQ**), CN (**CNFQ**), $COCH_3$, (**ACFQ**), Fig. 1, were synthesized and purified in our laboratory as described in [67]. The spin trapping agent, 5,5-dimethyl-1-pyrroline *N*-oxide (DMPO; Aldrich) was distilled before application and stored at −18 °C. The production of singlet oxygen was confirmed by EPR *via* oxidation of 4-hydroxy-2,2,6,6-tetramethylpiperidine (TMP; Merck-Schuchardt) to paramagnetic 4-hydroxy-2,2,6,6-tetramethylpiperidine *N*-oxyl (TEMPOL). The concentration of photogenerated paramagnetic species was determined using solutions of 4-hydroxy-2,2,6,6-tetramethylpiperidine *N*-oxyl (TEMPOL; Aldrich) as calibration standards. Dimethylsulfoxide (SeccoSolv® Merck), acetonitrile (SeccoSolv® Merck) and 1,4-dioxane (DIOX, Uvasol®, Merck) were used as aprotic solvents. Sodium azide (analytical grade, Sigma–Aldrich) was applied as selective singlet oxygen quencher.

2.3. Experimental methods and apparatus

2.3.1. UV/vis experiments

UV/vis spectra of the investigated fluoroquinolones in ACN, DMSO and DIOX solvents were recorded using a UV-3600 UV/vis spectrometer (Shimadzu, Japan) with 1 cm square quartz cell. The UV/vis spectra of fluoroquinolones in ACN in the presence of TMP (identical composition as used in EPR experiments) were measured using 0.2 cm quartz cell.

2.3.2. EPR in situ photochemical experiments

The formation of paramagnetic intermediates upon UV irradiation of fluoroquinolones in DMSO was monitored by EPR spin trapping technique using DMPO. The photoinduced production of singlet oxygen during excitation of fluoroquinolones was measured in ACN solutions with TMP [68–71]. The solutions of fluoroquinolone derivatives containing DMPO or TMP prepared immediately before the EPR measurements were carefully mixed by a slight air stream and immediately transferred to a small quartz flat cell (WG 808-Q, Wilmad-LabGlass, USA; optical cell length 0.04 cm) optimized for the TE_{102} cavity. The samples were irradiated at 295 K directly in the EPR resonator, and EPR spectra were recorded *in situ*. As an irradiation source an HPA 400/30S lamp (400 W, Philips) was used [68]. The UVA irradiance of the UV lamp, 5.5 mW cm^{-2}, within the EPR cavity was determined using a UVX radiometer (UVP, USA). The concentration of photogenerated paramagnetic species was evaluated from double-integrated EPR spectra using the calibration curve obtained by EPR spectra of TEMPOL.

Typical EPR spectrometer settings in a standard photochemical experiment were: microwave frequency, 9.44 GHz; microwave power, 10.03 mW; center field, 335.0 mT; sweep width, 10 mT; gain, 5×10^5; modulation amplitude, 0.05–0.1 mT; scan, 20.97 or 41.94 s; time delay, 1.03 or 3.06 s; time constant, 5.12 or 20.48 ms. The *g*-values were determined with an uncertainty of ±0.0001 by simultaneous measurement of a reference standard containing DPPH. Detected EPR spectra were analyzed and simulated by the Bruker software WinEPR and SimFonia and the Winsim2002 software free available from the website of National Institute of Environmental Health Sciences (NIEHS) (http://epr.niehs.nih.gov/) [72].

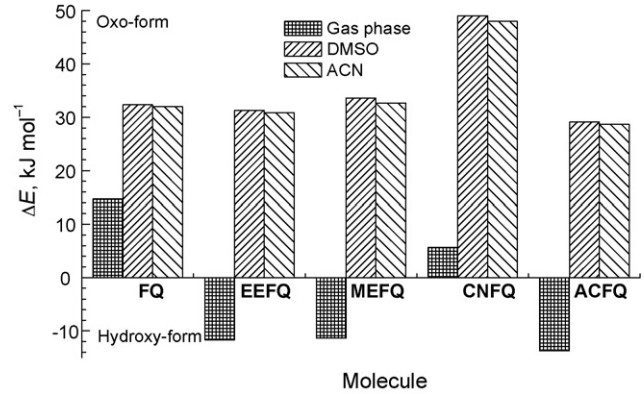

Fig. 2. Differences between the ZPE corrected B3LYP total energies of hydroxy and oxo forms of the investigated fluoroquinolone derivatives in the gas phase and aprotic solvents.

3. Results and discussion

3.1. Optimized geometries

The investigated fluoroquinolones exhibit two types of structural forms [73,74]. The first, original structure, represents the oxo-tautomer, while the second, hydroxy-tautomer, is the result of 1,5-hydrogen shift from N1 atom to oxygen in position 4 (Eq. (1)).

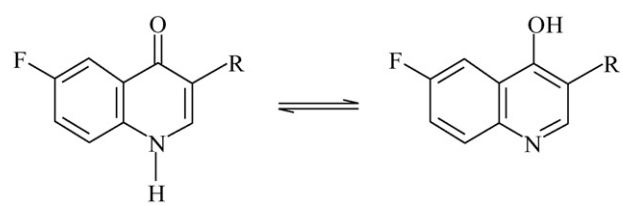

(1)

Gas-phase B3LYP/6-31+G(d) calculations with inclusion of the Zero Point Energy (ZPE) corrections indicate that the hydroxy-tautomer is preferred in the case of **EEFQ**, **MEFQ** and **ACFQ** molecules as shown in Fig. 2. The presence of hydrogen intramolecular interaction between the OH group and oxygen atom of the neighboring substituent R stabilizes this structure by approximately 13 kJ mol^{-1}. Solution-phase calculations using the IEF-PCM method showed that a solvent has a dramatic influence on the population of oxo-tautomers in the solution. Although the energy differences between the oxo- and hydroxy-tautomers of studied molecules are very small (from 0.1 to 0.8 kJ mol^{-1}) in the two investigated solvents, in DMSO the oxo-tautomer is slightly preferred in comparison to ACN.

According to the atom numbering in Fig. 1, the optimal gas phase bond lengths in rings are compiled in supplement Table S1. Significant differences between the two tautomeric forms are found for the bond N1–C2, C2–C3, C3–C4 and C9–C10 lengths. These changes are related to the aromatic character of the hydroxy-tautomer ring. The substituents affect the C2–C3 and C3–C4 bonds significantly (bonds in the vicinity of the substituent). Consequently, these bonds are elongated for both molecular forms with respect to the pristine **FQ** molecule and the changes found are in the 0.013–0.017 Å range. These elongations are compensated with the shortening of the C9–C10 bonds of the quinolone skeleton; for the oxo-tautomer, these changes are up to 0.105 Å. The effect of the substituent is also observed for the C4=O and C4–O bonds. Values in Table S1 indicate that COOR (**EEFQ** and **MEFQ**) and cyano (**CNFQ**) groups cause a shortening of the C4=O or C4–O bonds in the two investigated forms.

Table 1
TD-DFT and RI-CC2 singlet excitation energies (in eV) and oscillator strengths (f) of the first three dominant electronically excited states $E(S_i)$, $i = 1–3$.

Environment	Derivative				
	FQ	**EEFQ**	**MEFQ**	**CNFQ**	**ACFQ**
Oxo-form					
Gas phase	4.05 (0.105)[a]	4.13 (0.093)[a]	4.13 (0.094)[a]	4.06 (0.094)[a]	4.09 (0.124)[b]
	4.68 (0.049)	4.31 (0.187)	4.31 (0.183)	4.37 (0.153)	4.18 (0.151)
	5.37 (0.169)	5.14 (0.098)	5.15 (0.094)	5.06 (0.137)	5.06 (0.092)
Gas phase, RI-CC2	4.14 (0.153)	4.24 (0.119)	4.25 (0.119)	4.22 (0.135)	4.22 (0.127)
	4.90 (0.108)	4.54 (0.277)	4.54 (0.274)	4.62 (0.234)	4.39 (0.271)
	5.59 (0.136)	5.51 (0.128)	5.52 (0.129)	5.51 (0.069)	5.42 (0.105)
DMSO	4.00 (0.163)	4.12 (0.096)[a]	4.13 (0.095)[a]	4.10 (0.113)	4.01 (0.268)[a]
	4.62 (0.038)	4.21 (0.300)	4.22 (0.294)	4.29 (0.231)	4.12 (0.125)
	5.18 (0.140)	5.07 (0.271)	5.07 (0.280)	5.05 (0.380)	4.97 (0.166)
ACN	4.02 (0.150)	4.13 (0.087)[a]	4.14 (0.086)[a]	4.11 (0.103)	4.02 (0.260)[b]
	4.63 (0.034)	4.22 (0.280)	4.23 (0.276)	4.30 (0.210)	4.13 (0.115)
	5.19 (0.101)	5.08 (0.247)	5.08 (0.252)	5.06 (0.347)	4.97 (0.151)
Hydroxy-form					
Gas phase	4.30 (0.062)	3.92 (0.046)	3.91 (0.047)	4.05 (0.042)	3.69 (0.057)
	5.58 (0.037)	5.20 (0.920)	5.20 (0.903)	5.31 (0.636)	4.94 (0.651)
	5.80 (0.952)	5.35 (0.124)	5.35 (0.124)	5.50 (0.464)	5.13 (0.166)
Gas phase, RI-CC2	4.96 (0.107)	4.15 (0.038)	4.15 (0.040)	4.24 (0.029)	4.10 (0.037)
	6.08 (0.928)	4.92 (0.072)	4.92 (0.075)	4.89 (0.066)	4.91 (0.141)
	6.22 (0.242)	5.53 (0.862)	5.53 (0.845)	5.73 (1.001)	5.43 (0.793)
DMSO	4.27 (0.111)	3.93 (0.073)	3.92 (0.075)	4.01 (0.072)	3.69 (0.086)
	5.48 (0.387)	5.04 (1.283)	5.04 (1.271)	5.14 (1.301)	4.82 (0.985)
	5.57 (0.796)	5.47 (0.133)	5.46 (0.128)	5.37 (0.135)	5.10 (0.076)
ACN	4.28 (0.102)	3.94 (0.066)	3.93 (0.068)	4.02 (0.066)	3.70 (0.079)
	5.49 (0.184)	5.07 (1.223)	5.07 (1.212)	5.18 (1.204)	4.85 (0.930)
	5.60 (0.940)	5.48 (0.121)	5.47 (0.116)	5.38 (0.173)	5.11 (0.085)

[a] The first relevant singlet excited state is S_2 state.
[b] The first relevant singlet excited state is S_3 state.

3.2. Spectroscopic properties

The structural changes induced by the studied electron-withdrawing groups are also reflected in the vertically excited singlet electronic states. The first three vertical excitation energies with non-negligible oscillator strengths ($f > 0.03$) are summarized in Table 1. In the case of hydroxy-tautomers of studied quinolones, in all environments the lowest excited state S_1 has non-negligible oscillator strength. Calculated excitation energies lie in the range from 3.69 to 4.30 eV. In oxo-tautomers, the majority of first relevant singlet excited states is the S_2 state. For **ACFQ** we found that first relevant singlet excited state in gas phase and ACN solution is the S_3 state (Table 1). However all these values are in narrow interval from 4.00 to 4.25 eV.

If we compare the first TD-DFT excitation energy for the oxo-tautomers in the gas phase, the pristine molecule **FQ** has the lowest value. Substitution leads to the increase in excitation energy by 0.08 eV for **EFFQ**. On the other hand, substitutions in the hydroxy-tautomers induce the opposite effect. The addition of electron-withdrawing groups (except for CN group) allowing the formation of hydrogen bonds between the O–H groups leads to a decrease in the first excitation energy. The maximal decrease, 0.38 eV, is predicted for the **EEFQ** molecule. The effect of substitution is also apparent for the second and third relevant excitation energies. For both molecular forms, these energies are significantly closer to the first transition in comparison to the non-substituted **FQ** molecule. Confrontation with reference *ab initio* calculation results for gas-phase shows that the RI-CC2 gives higher excitation energies than TD-DFT but the overall trends are similar. If we compare the excitation energies obtained using the IEF-PCM model, these are shifted by 0.05–0.03 eV with respect to the gas phase. The presence of the solvent causes small changes in oscillator strengths (Table 1), too.

For all studied molecules in the two forms, the first lowest energy transitions are connected with the electron excitation from the highest occupied (HOMO) to the lowest unoccupied (LUMO) molecular orbital. The shape of orbitals is practically identical in all molecules, i.e. independent on the substituent. The HOMO and LUMO orbitals are delocalized over the molecule (see supplement Fig. S1 for **FQ** molecule). The HOMO–LUMO excitation has π–π^* character and includes electron transfer from the fluorine atom towards the π-system. In both forms it also includes the transfer from oxygen atom.

Table 2 presents three lowest vertical triplet excitation energies of studied molecules in the gas- and solution-phase obtained from TD-DFT calculations. The data in Table 2 evidence that the environment has a negligible effect on the first excited triplet, T_1, state. For all molecules, T_1 vertical excitation energies are lower for the hydroxy-tautomers. Values in Table 2 also reveal that there is no substantial difference between T_1 vertical excitation energies of the individual molecules under study.

Sufficient energy gap between the first and second excited triplet state enables to restrict our considerations for the thermodynamics of ROS formation (see Section 3.4) to the first excited triplet state T_1.

The experimental UV/vis spectra of the investigated fluoroquinolone derivatives in ACN (dielectric constant 37.5; 20 °C), along with their simulated TD-DFT B3LYP/6-31+G(d) theoretical electron absorption spectra of oxo- and hydroxy-tautomers are shown in Fig. 3. Theoretical spectra of the oxo- and hydroxy-tautomer were constructed from the first 15 vertical excitations and their transition dipole moments using the program Orca_Asa [75,76], a general efficient quantum chemical method for predicting absorption bandshapes, resonance Raman spectra and excitation profiles for larger molecules. Gaussian broadening with HWHH of 1500 cm^{-1} was used. The resulting intensity of the hydroxy-

Table 2
Three lowest TD-DFT triplet excitation energies, $E(T_i)$/eV, $i = 1–3$.

Environment	Derivative				
	FQ	**EEFQ**	**MEFQ**	**CNFQ**	**ACFQ**
Oxo-form					
Gas phase	2.90	3.07	3.07	2.96	3.03
	3.32	3.27	3.27	3.33	3.25
	3.50	3.35	3.35	3.41	3.35
DMSO	2.89	3.11	3.12	3.07	3.12
	3.59	3.37	3.37	3.39	3.19
	3.74	3.57	3.54	3.67	3.55
ACN	2.89	3.11	3.12	3.07	3.12
	3.59	3.37	3.37	3.39	3.19
	3.73	3.57	3.53	3.67	3.55
Hydroxy-form					
Gas phase	2.82	2.79	2.79	2.76	2.74
	3.96	3.54	3.53	3.66	3.26
	4.05	3.77	3.77	3.74	3.44
DMSO	2.83	2.81	2.81	2.79	2.74
	3.98	3.57	3.56	3.65	3.36
	4.07	3.79	3.79	3.77	3.60
ACN	2.83	2.81	2.81	2.79	2.74
	3.98	3.57	3.56	3.65	3.36
	4.07	3.79	3.79	3.77	3.60

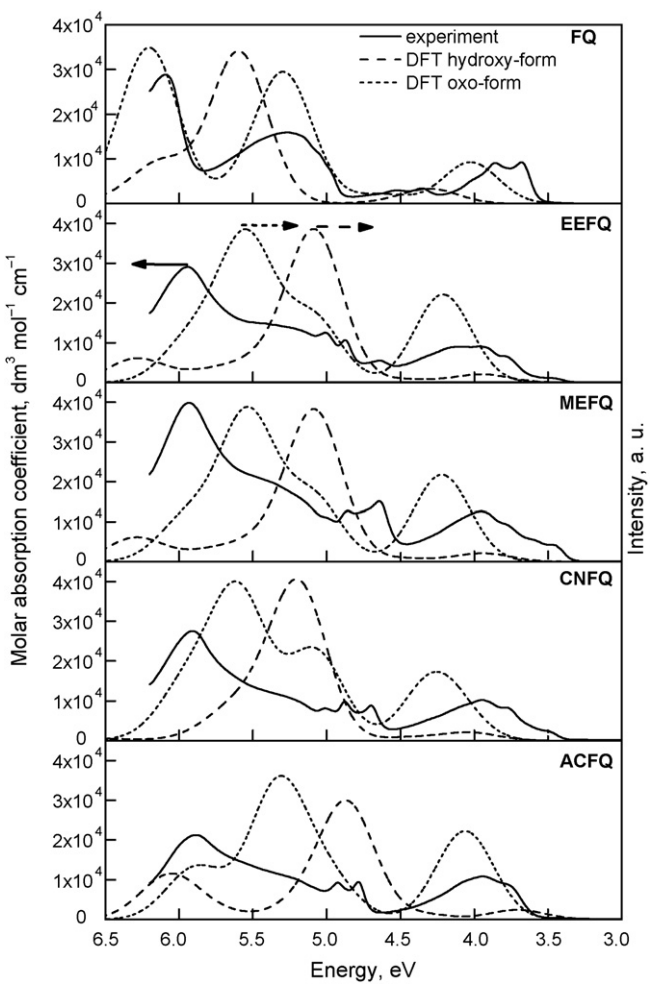

Fig. 3. Experimental UV/vis spectra of studied molecules in ACN. The simulated TD-DFT(IF-PCM=ACN)/6-31+G(d) spectra of studied molecules in oxo- and hydroxy-form. Theoretical absorption intensities (right *y*-axis) are in arbitrary units (a.u.).

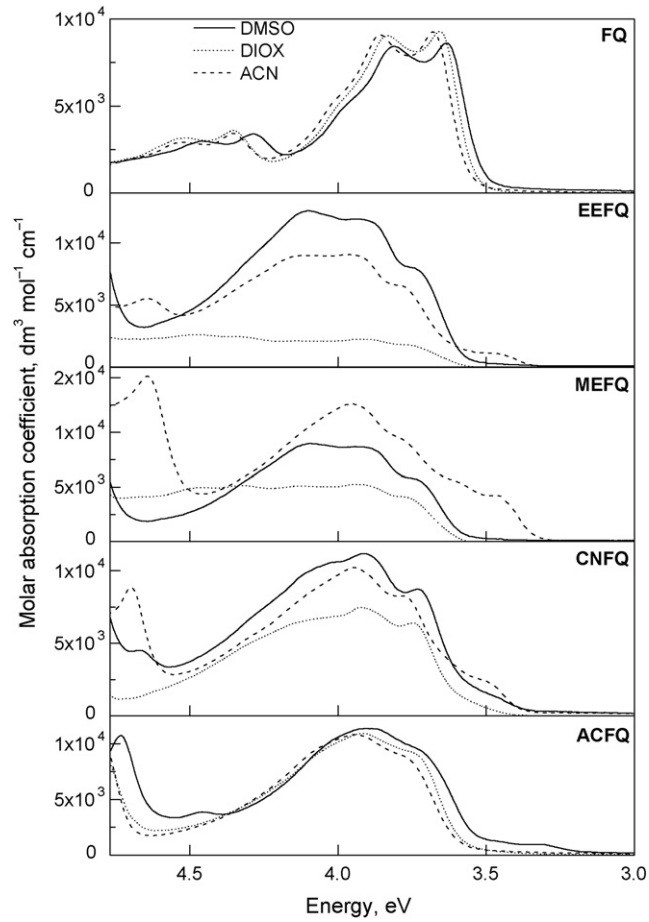

Fig. 4. Experimental UV/vis spectra of studied molecules in ACN, DMSO and DIOX.

tautomer has been divided by a factor of 2 to compare the intensity of the first excitation on molecule **FQ** with the experimental spectrum. Besides, the UV/vis spectra measured in ACN, DMSO (dielectric constant 47; 20 °C) and DIOX (dielectric constant 2.21; 20 °C) are depicted in Fig. 4. The characteristic UV/vis absorptions of investigated fluoroquinolone derivatives in ACN, DMSO and DIOX solvents extracted from experimental spectra are summarized in Table 3.

According to the literature data oxo-tautomer represents the preferred structure of 4-oxoquinoline molecule in polar solvents and crystalline state. The decrease in solvent polarity causes an increase in hydroxy-tautomer concentration [73,77–80]. However, the hydroxy-tautomer can be stabilized also in polar media when hydrogen bond acceptors are present at position 3 of 4-oxoquinoline skeleton [67]. It is well known that experimental UV/vis spectra of 4-hydroxyquinolines show intensive absorption in the spectral region 260–290 nm (4.77–4.28 eV), and only negligible absorption in the region 310–360 nm (4.0–3.44 eV) can be found [81].

Our UV/vis spectra of fluoroquinolone derivatives obtained in ACN are in good accordance with the coincident presence of oxo- and hydroxy-tautomers. This conclusion is also supported with spectra calculations, despite of hypsochromic shifts observed for calculated absorption bands using TD-DFT B3LYP/6-31+G(d) method (Fig. 3). The first band splitting-off in the UV/vis spectrum of **FQ** represents an often observed behavior of such quinoline compounds [14,82,83] and it can be assigned mainly to C–C and C–N skeleton vibrations of the quinolone moiety. The B3LYP/6-31+G(d) normal modes of the C–C vibrations were found around 1223 and 1397 cm^{-1}, while the in-plane skeleton vibrations including the NH

Table 3
Characteristic UV/vis absorptions of investigated fluoroquinolone derivatives in aprotic solvents with the corresponding values of molar absorption coefficients.

Derivative	Environment					
	ACN		DMSO		DIOX	
	E_{max}, eV	ε_{max}, M^{-1} cm^{-1}	E_{max}, eV	ε_{max}, M^{-1} cm^{-1}	E_{max}, eV	ε_{max}, M^{-1} cm^{-1}
FQ	6.08	28 700	–	–	–	–
	5.25	13 800	–	–	–	–
	4.53	2900	4.46	3000	4.51	3200
	4.35	3400	4.28	3400	4.35	3600
	3.85	9100	3.82	8400	3.83	9100
	3.68	9300	3.63	8600	3.66	9300
EEFQ	5.93	29 000	–	–	4.86	3500
	5.00	12 600	–	–	4.48	2600
	4.86	10 500	–	–	4.34	2500
	4.12	9000	4.11	12 500	4.13	2100
	3.96	9050	3.94	11 800	3.92	2200
	3.78	6500	3.75	7900	3.76	1800
MEFQ	–	–	–	–	4.86	6700
	5.93	39 800	–	–	4.46	5000
	4.86	12 700			4.32	5200
	4.64	14 900	4.09	9000	4.13	5200
	3.94	12 600	3.91	8600	3.94	5300
	3.73	8600	3.75	5800	3.76	4100
CNFQ	5.91	27 500	–	–	–	–
	5.00	8100	–	–	4.86	4500
	4.88	9800	4.09	9900	4.13	6300
	3.95	10 200	3.91	11 000	3.91	7300
	3.78	8200	3.72	8500	3.75	6300
ACFQ	5.88	21 200	–	–	–	–
	4.92	9300	–	–	–	–
	4.79	9500	–	–	4.79	8500
	3.94	10 800	3.91	11 200	3.91	11 000
	3.77	8750	3.73	9500	3.76	9300

group lie at 1548, 1597, 1616 and 1670 cm^{-1}. Taking into account a scaling factor of ~0.96 for the B3LYP/6-31+G(d) method, this data agrees with the experimental splitting-off (approx. 0.17 eV) for the pristine molecule **FQ** well.

Replacement of ACN by more polar DMSO solvent caused only small variations in the UV/vis absorption characteristics of investigated fluoroquinolones (Table 3). However, when UV/vis spectra were measured in DIOX representing non-polar aprotic solvent, significant changes were observed especially for **EEFQ**, **MEFQ** and **CNFQ** derivatives, reflecting the increase of hydroxy-tautomer concentrations (Fig. 4 and Table 3). Comparison of experimental solution-phase spectra with theoretical spectra of the two tautomeric forms gives evidence that in solutions studied quinolones are present in both forms.

TD-B3LYP/6-311++G(2df,2pd) vertical excitation energies for **FQ** molecule were slightly lower than the values obtained for the 6-31+G(d) basis set. It indicates that the larger size of employed basis set does not influence vertical excitation energies significantly. Similar results were obtained using aug-cc-pVDZ, and aug-cc-pVTZ basis sets. Using the TD-PBE0/6-31+G(d) approach

Table 4
Vertical electron affinities (VEA) and vertical ionization potentials (VIP) in eV of the studied molecules for S_0, T_1 and S_1 states.

Environment	Gas phase					DMSO[a]					ACN[a]				
Derivative	**FQ**	**EEFQ**	**MEFQ**	**CNFQ**	**ACFQ**	**FQ**	**EEFQ**	**MEFQ**	**CNFQ**	**ACFQ**	**FQ**	**EEFQ**	**MEFQ**	**CNFQ**	**ACFQ**
Oxo-form															
VEA(S_0)	0.08	0.29	0.31	0.67	0.33	1.91	1.98	2.02	2.18	2.03	1.48	2.04	2.00	2.17	2.02
VEA(T_1)[b]	2.98	3.36	3.38	3.63	3.36	4.80	5.09	5.14	5.25	5.15	4.37	5.15	5.12	5.24	5.14
VEA(S_1)[c]	4.12	4.42	4.44	4.74	4.42	5.91	6.10	6.15	6.29	6.04	5.51	6.17	6.14	6.29	6.04
VIP(S_0)	8.07	8.20	8.24	8.53	8.32	6.05	6.30	6.35	6.46	6.34	6.67	6.89	6.36	6.47	6.35
VIP(T_1)[d]	5.17	5.13	5.17	5.57	5.29	3.16	3.19	3.23	3.39	3.22	3.78	3.78	3.24	3.40	3.23
VIP(S_1)[e]	4.02	4.07	4.10	4.47	4.23	2.05	2.18	2.22	2.36	2.34	2.65	2.76	2.22	2.36	2.33
Hydroxy-form															
VEA(S_0)	0.02	0.61	0.65	0.86	0.26	1.85	2.36	2.37	2.41	2.59	2.25	2.27	2.36	2.40	2.58
VEA(T_1)[b]	2.84	3.40	3.44	3.62	3.00	4.68	5.17	5.18	5.20	5.33	5.08	5.08	5.17	5.19	5.32
VEA(S_1)[c]	4.32	4.53	4.55	4.91	3.94	6.12	6.29	6.29	6.43	6.28	6.53	6.21	6.29	6.42	6.28
VIP(S_0)	8.31	8.37	8.42	8.80	9.09	6.30	6.58	6.58	6.67	6.58	5.71	6.01	6.59	6.68	6.59
VIP(T_1)[d]	5.49	5.58	5.63	6.04	6.35	3.47	3.77	3.77	3.88	3.84	2.88	3.20	3.78	3.89	3.85
VIP(S_1)[e]	4.01	4.45	4.51	4.75	5.40	2.03	2.65	2.66	2.66	2.89	1.43	2.07	2.66	2.66	2.89

[a] In solution-phase VIPs and VEAs the energy of electron solvation is not included. Its inclusion lowers VIP and VEA values by 0.84 eV in DMSO and by 0.95 eV in ACN.
[b] $VEA(T_1) = VEA(S_0) + {}^3E_{0-0}$.
[c] $VEA(S_1) = VEA(S_0) + {}^1E_{0-0}$.
[d] $VIP(T_1) = VIP(S_0) - {}^3E_{0-0}$.
[e] $VIP(S_1) = VIP(S_0) - {}^1E_{0-0}$.

we obtained vertical excitation energies of studied molecules in ACN in better agreement with experimental spectra in comparison to TD-B3LYP/6-31+G(d) results. PBE0 excitation energies are by 0.1–0.25 eV higher than B3LYP ones. However, the shape and trends in the obtained spectra are analogous for the two functionals.

Obtained results show that in studied solvents both forms of studied quinolones are simultaneously present. However, the solvent is able to modify the ratio between oxo- and hydroxy-tautomer concentrations.

3.3. Ionization potentials and electron affinities of quinolones in ground and excited states

Vertical ionization potentials (VIPs) of studied molecules in oxo- and hydroxy-forms were calculated as the difference in the total electronic energies of the radical cation, $E(M^{\bullet+})$, and its parent neutral molecule, $E(M)$

$$\mathrm{VIP} = E(M^{\bullet+}) - E(M) \quad (2)$$

The energy of radical cation $M^{\bullet+}$ was computed for the geometry identical with the parent molecule M. Vertical electron affinities (VEA) were computed as the difference in the energies of parent molecule M and the corresponding radical anion $M^{\bullet-}$

$$\mathrm{VEA} = E(M) - E(M^{\bullet-}) \quad (3)$$

This quantity corresponds to the negative energy change related to the formation of the $M^{\bullet-}$ radical anion

$$M + e^- \rightarrow M^{\bullet-} \quad -\mathrm{VEA} \quad (4)$$

All calculated VIP and VEA values are compiled in Table 4. Used denotation S_1 refers to the lowest relevant excited singlet state which may not correspond to the actual first excited singlet state. (For the majority of molecules in the oxo-form, the lowest excited singlet state with non-negligible oscillator strength is the second one, see Table 1.) These results show that solvation of the studied species leads to VIPs lower usually by ca. 2 eV. VIPs are almost always lowest for **FQ** molecule. The highest ones were found mostly for **CNFQ** molecule. These results are in accordance with the fact that electron-withdrawing groups induce an increase in ionization potential [84].

VEA values in Table 4 show the energy liberated when a molecule in ground or excited state accepts the electron. The lowest energy change shows **FQ** molecule in both tautomeric forms and the highest energy change was found mostly for **CNFQ** molecule.

Data in Table 4 show that solvents induce a drop in ionization potential and an increase in electron affinities of the studied molecules. Electron transfer from these molecules in solution-phase therefore requires less energy. Simultaneously, these molecules have a higher ability to act as electron acceptors in comparison to gas phase.

In general, gas-phase vertical ionization potential represents the energy difference between the radical cation and the parent molecule. Energy of the released electron is considered zero, because the process represents the removal of the electron from a molecule to infinite distance. In order to assess the effect of the solvent on the VIP values, the solution-phase VIPs were determined the same way (Eq. (2)). Inclusion of the solvation energy of electron, which is negative [85] will lead to lower VIP and VEA values (by 0.84 eV in DMSO and by 0.95 eV in ACN). In this study we did not involve the electron solvation energy for the evaluation of energy requirements of processes described in Eqs. (5)–(8), because the contributions of electron solvation are canceled in the calculated VIP–VEA differences.

In order to discuss the energetics of the possible reaction mechanisms, the lowest electronic excitation energies and one-electron properties of molecular oxygen in vacuum, dimethylsulfoxide (DMSO) and acetonitrile (ACN) were also calculated (Table 5). As it can be seen in Table 5, the computed excitation energies for the lowest optical transitions in the gas phase are 1.07 and 1.67 eV in good accordance with the experimental values 0.98 and 1.64 eV [86], respectively. The calculated adiabatic electron affinity (AEA) is 0.59 eV, the experimental value is 0.45 eV [87]. The calculated adiabatic ionization potential (AIP) is 12.63 eV. It agrees with the experimental 12.07 eV value [86] very well. The effect of solvation (in DMSO and ACN) causes a lowering of the ionization potential (VIP and AIP) by 3.5 eV (see Table 5). The identical solvent effect on the mentioned quantities was reported by Llano et al. [88] at the B3LYP/6-31G(d,p)//B3LYP/6-31G(d,p) level of theory in the water. It should be noted that the most accurate treatment of the molecular oxygen singlet states requires application of computationally demanding *ab initio* multi-configuration approach.

Table 5
Computed lowest singlet excitation energies $E_{S,1}(O_2)$[a], $E_{S,2}(O_2)$[b] and one-electron properties of molecular oxygen in vacuum, DMSO and ACN. All values are in eV.

Environment	$E_{S,1}(O_2)$	$E_{S,2}(O_2)$	VIP(O_2)	AIP(O_2)	VEA(O_2)	AEA(O_2)
Vacuum	1.07 0.98[c]	1.67 1.64[c]	11.48	12.63 12.07[c]	1.76	0.59 0.45[d]
DMSO	1.06	1.64	7.94	9.11	4.98	3.83
ACN	1.06	1.64	7.96	9.13	4.96	3.81

[a] $^3\Sigma_g^- \rightarrow {}^1\Delta_g$ excitation.
[b] $^3\Sigma_g^- \rightarrow {}^1\Sigma_g^+$ excitation.
[c] Experimental value [86].
[d] Experimental value [87].

3.4. Energetics of various mechanisms of $O_2^{\bullet-}$ and singlet oxygen formation

The superoxide radical anion may be produced by direct electron transfer between the fluoroquinolone molecule M in excited triplet (T_1) or singlet (S_1) state and $^3O_2$

$$M(T_1) + O_2(^3\Sigma_g^-) \rightarrow M^{\bullet+} + O_2^{\bullet-} \qquad \Delta E_{TO} = \mathrm{VIP}(T_1) - \mathrm{VEA}(O_2) \quad (5)$$

$$M(S_1) + O_2(^3\Sigma_g^-) \rightarrow M^{\bullet+} + O_2^{\bullet-} \qquad \Delta E_{SO} = \mathrm{VIP}(S_1) - \mathrm{VEA}(O_2) \quad (6)$$

The energetics of these processes can be described as the difference in the ionization potential of the fluoroquinolone in the excited state and the electron affinity of $^3O_2$. Again, for the sake of denotation simplicity, in Eqs. (5)–(8) and Fig. 5, S_1 refers to the first *relevant* excited singlet state.

The computed vertical electron affinity of molecular oxygen VEA(O_2) for the gas phase reached 1.76 eV (Table 5). In the aprotic solvents DMSO and ACN, this value is higher by ca. 3.2 eV.

The VIP(T_1) and VIP(S_1) values of the investigated fluoroquinolone derivatives in the two tautomeric forms are summarized in Table 4. These values are lower than VEA(O_2) in both solvents. Therefore, in DMSO and ACN solutions, excited fluoroquinolones are able to transfer the electron to the molecular oxygen. In the case of process (5), the energy differences ΔE_{TO} reached values from −1.07 to −2.08 eV. For process (6), ΔE_{SO} values are larger, from −2.09 to −3.53 eV. In the case of DMSO, process (5) is more favorable for oxo-tautomers. In ACN solutions, such an unambiguous conclusion is not possible. For **FQ** and **EEFQ** molecules, electron transfer from T_1 state of hydroxy-tautomer is thermodynamically preferred. For **MEFQ**, **CNFQ** and **ACFQ**, reaction of the oxo-tautomer is favored. If we consider process (6), analogous conclusions can be drawn.

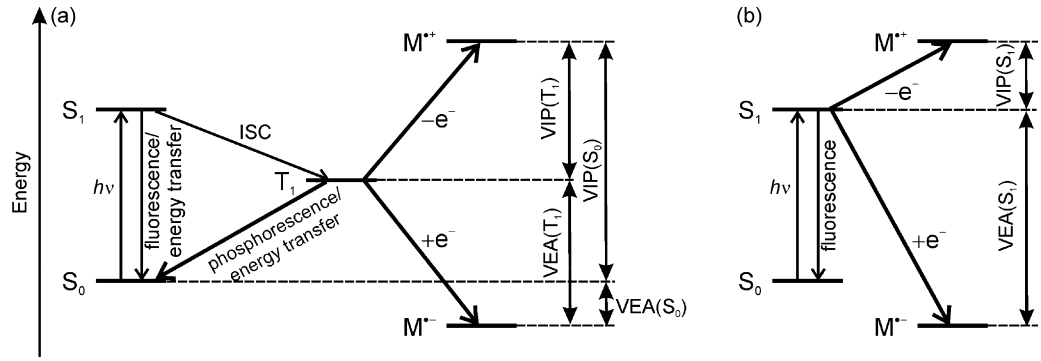

Fig. 5. Schematic illustration of photoinduced processes of molecule M upon absorption of UVA radiation.

Processes (5) and (6) are not favored in the gas phase, where VEA(O_2) is lower and the ionization potentials VIP(T_1) and VIP(S_1) are significantly higher than corresponding solution-phase values.

Because the species involved in processes (5) and (6) may undergo geometry relaxation, we have also evaluated ΔE_{TO} and ΔE_{SO} for adiabatic ionization potentials, AIP(T_1) and AIP(S_1), and electron affinity, AEA(O_2). Obtained adiabatic ΔE_{TO} and ΔE_{SO} values are higher in comparison to the vertical ones. Average deviation between the vertical and adiabatic energies reached ca. 1 eV (data not shown). In solution-phase, the resulting values are still negative.

Photoinduced (indirect) $O_2^{\bullet-}$ production may also involve initial electron transfer from photoexcited fluoroquinolone molecule in singlet or triplet state to an electron donor (D), forming the corresponding radical cation ($M^{\bullet+}$) and radical anion ($D^{\bullet-}$). The latter subsequently reacts with molecular oxygen to produce superoxide radical anion [89,90]. We assume that the fluoroquinolones in excited T_1 or S_1 states (Fig. 5) may play simultaneously the role of the electron donor (autoionization processes [88]). The solution-phase VIP(T_1) energies of fluoroquinolones are in the range from 2.88 to 3.88 eV. Their electron affinities VEA(T_1) are from 4.37 to 5.32 eV (Table 4). The VIP(S_1) values were found in the range from 1.43 to 2.89 eV, and the VEA(S_1) lie between 5.51 and 6.53 eV (Table 4). Data in this table and Fig. 5a demonstrate that interaction between the molecules in ground S_0 state and excited state is not favored from the thermodynamics point of view. This is in accordance with the well-known fact that the molecule in excited state is a better oxidizing and simultaneously better reducing agent than the molecule in the ground state. Table 6 summarizes changes in the energy related to the formation of radical cation and radical anion from the lowest triplet and singlet excited states

$$M(T_1) + M(T_1) \rightarrow M^{\bullet+} + M^{\bullet-} \qquad \Delta E_{TT} = VIP(T_1) - VEA(T_1) \tag{7}$$

$$M(S_1) + M(S_1) \rightarrow M^{\bullet+} + M^{\bullet-} \qquad \Delta E_{SS} = VIP(S_1) - VEA(S_1) \tag{8}$$

From this table, it is clear that these two processes are thermodynamically favorable in solution-phase because ΔE_{TT} and ΔE_{SS} are negative. In agreement with Fig. 5, thermodynamically more effective is the interaction of two S_1 states. In DMSO, reaction (7) is thermodynamically preferred for oxo-tautomers of the studied quinolones. In ACN, the same process is preferred for oxo-tautomers in the case of **MEFQ**, **CNFQ** and **ACFQ**. Analogous conclusions hold up for reaction (8), with exception for **FQ** molecule, where ΔE_{SS} is significantly lower for the hydroxy-tautomer. In the gas phase, formation of $M^{\bullet+}$ and $M^{\bullet-}$ from the molecules in T_1 state requires an additional energy, $\Delta E_{TT} > 0$.

In the second step, electron transfer from $M^{\bullet-}$ occurs

$$M^{\bullet-} + O_2 \rightarrow M + O_2^{\bullet-} \qquad \Delta E_{et} = VEA(S_0) - VEA(O_2) \tag{9}$$

Energy change, ΔE_{et}, corresponding to this process can be expressed in terms of quinolone and O_2 vertical electron affinities VEA(S_0) and VEA(O_2), respectively. Again, negative ΔE_{et} values shown in Table 6 indicate that the process (9) is thermodynamically favored. In ACN solutions, reaction of hydroxy-tautomers of investigated quinolones is thermodynamically preferred. In DMSO, the reaction of oxo-tautomers is more favorable, with exception of **FQ** molecule. In the gas phase, electron transfer (9) is favored from the thermodynamics point of view, too.

Energy transfer from quinolone in S_1 and T_1 states to O_2 and formation of $^1\Delta_g$ singlet oxygen represents another pathway of ROS formation. Here, the deexcitation energies, $E(S_1)$ or $E(T_1)$, should be

Table 6
Energy changes related to the processes described in Eqs. (7)–(10) in eV.

Environment	Gas phase					DMSO					ACN				
Derivative	**FQ**	**EEFQ**	**MEFQ**	**CNFQ**	**ACFQ**	**FQ**	**EEFQ**	**MEFQ**	**CNFQ**	**ACFQ**	**FQ**	**EEFQ**	**MEFQ**	**CNFQ**	**ACFQ**
Oxo-form															
ΔE_{TT}	2.19	1.77	1.78	1.95	1.94	−1.64	−1.90	−1.90	−1.86	−1.92	−0.60	−1.36	−1.88	−1.84	−1.91
ΔE_{SS}	−0.10	−0.35	−0.34	−0.27	−0.20	−3.86	−3.92	−3.92	−3.93	−3.71	−2.86	−3.41	−3.92	−3.93	−3.71
ΔE_{et}	−1.68	−1.47	−1.45	−1.09	−1.43	−3.07	−3.00	−2.96	−2.80	−2.95	−3.48	−2.92	−2.96	−2.79	−2.94
$\Delta E_{T\rightarrow O}$	−1.83	−2.00	−2.00	−1.89	−1.96	−1.83	−2.05	−2.06	−2.01	−2.06	−1.83	−2.05	−2.06	−2.01	−2.06
$\Delta E_{S\rightarrow O}$	−2.98	−3.06	−3.07	−2.99	−3.03	−2.94	−3.06	−3.07	−3.04	−2.95	−2.96	−3.07	−3.08	−3.05	−2.96
Hydroxy-form															
ΔE_{TT}	2.65	2.18	2.20	2.42	3.35	−1.21	−1.40	−1.41	−1.32	−1.49	−2.20	−1.89	−1.39	−1.30	−1.47
ΔE_{SS}	−0.31	−0.08	−0.04	−0.15	1.45	−4.09	−3.64	−3.63	−3.77	−3.39	−5.10	−4.14	−3.63	−3.76	−3.39
ΔE_{et}	−1.74	−1.15	−1.11	−0.90	−1.50	−3.13	−2.62	−2.61	−2.57	−2.39	−2.71	−2.69	−2.60	−2.56	−2.38
$\Delta E_{T\rightarrow O}$	−1.75	−1.72	−1.72	−1.69	−1.67	−1.77	−1.75	−1.75	−1.73	−1.68	−1.77	−1.75	−1.75	−1.73	−1.68
$\Delta E_{S\rightarrow O}$	−3.23	−2.85	−2.84	−2.98	−2.62	−3.21	−2.87	−2.86	−2.95	−2.63	−3.22	−2.88	−2.87	−2.96	−2.64

Table 7
Experimental (—) and simulated (—) EPR spectra (SW = 8 mT) obtained upon UVA exposure of investigated fluoroquinolone derivatives in DMSO/DMPO/air systems (exposure 660 s; c_0 = 3.2 mM; $c_{0,DMPO}$ = 0.04 M).

Derivative	Experimental and simulated EPR spectrum	Spin Hamiltonian parameters of simulations (hfcc in mT)
FQ	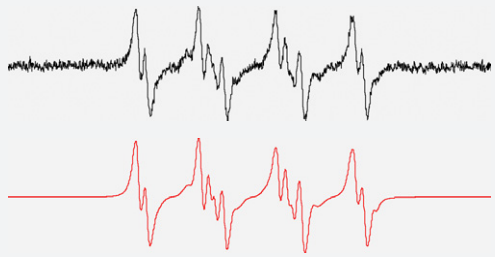	•DMPO-O_2^-: a_N = 1.275, a_H^β = 1.036, a_H^γ = 0.139, g = 2.0058, relative concentration 68%; •DMPO-OCH_3: a_N = 1.324, a_H^β = 0.822, a_H^γ = 0.196, g = 2.0059, 22%; •DMPO-OR: a_N = 1.417, a_H^β = 1.179, g = 2.0059, 10%.
EEFQ	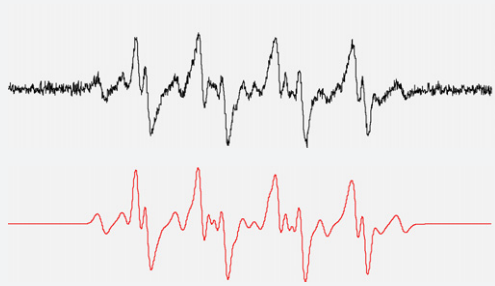	•DMPO-O_2^-: a_N = 1.275, a_H^β = 1.036, a_H^γ = 0.139, g = 2.0058, 53%; •DMPO-OCH_3: a_N = 1.324, a_H^β = 0.822, a_H^γ = 0.196, g = 2.0059, 25%; •DMPO-NR_1: a_N(NO) = 1.279, a_H^β = 1.564, a_N = 0.405, g = 2.0058, 22%.
MEFQ	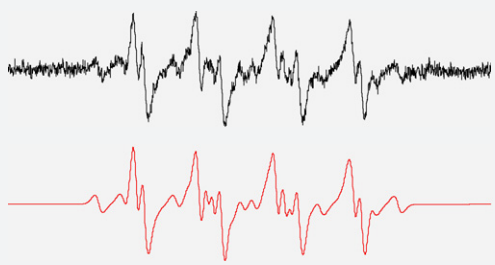	•DMPO-O_2^-: a_N = 1.275, a_H^β = 1.036, a_H^γ = 0.139, g = 2.0058, 48%; •DMPO-OCH_3: a_N = 1.324, a_H^β = 0.822, a_H^γ = 0.196, g = 2.0059, 31%; •DMPO-NR_1: a_N(NO) = 1.279, a_H^β = 1.564, a_N = 0.405, g = 2.0058, 21%.
CNFQ	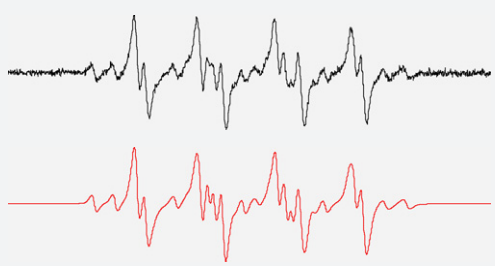	•DMPO-O_2^-: a_N = 1.275, a_H^β = 1.036, a_H^γ = 0.139, g = 2.0058, 64%; •DMPO-OCH_3: a_N = 1.324, a_H^β = 0.822, a_H^γ = 0.196, g = 2.0059, 24%; •DMPO-NR_2: a_N(NO) = 1.345, a_H^β = 1.771, a_N = 0.345, g = 2.0058, 12%.
ACFQ	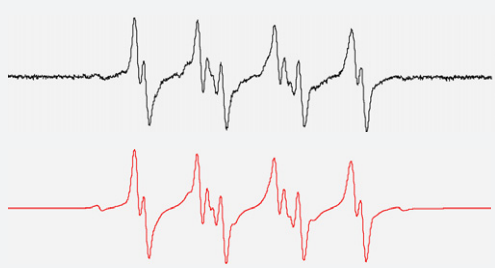	•DMPO-O_2^-: a_N = 1.275, a_H^β = 1.036, a_H^γ = 0.139, g = 2.0058, 53%; •DMPO-OCH_3: a_N = 1.324, a_H^β = 0.822, a_H^γ = 0.196, g = 2.0059, 37%; •DMPO-OR: a_N = 1.417, a_H^β = 1.179, g = 2.0058, 10%; 7%; •DMPO-CR: a_N = 1.457, a_H^β = 2.049, g = 2.0057, 2%.

compared with the excitation energy required for singlet oxygen ($^1\Delta_g$ state) formation, $E_{S,1}(O_2)$ [88]

$$M(T_1) + O_2(^3\Sigma_g^-) \rightarrow M(S_0) + O_2(^1\Delta_g)$$

$$\Delta E_{T\rightarrow O} = E_{S,1}(O_2) - E(T_1) \quad (10)$$

$$M(S_1) + O_2(^3\Sigma_g^-) \rightarrow M(S_0) + O_2(^1\Delta_g)$$

$$\Delta E_{S\rightarrow O} = E_{S,1}(O_2) - E(S_1) \quad (11)$$

Negative $\Delta E_{T\rightarrow O}$ and $\Delta E_{S\rightarrow O}$ values in Table 6 confirm that these processes are possible in all studied environments from the thermodynamics point of view.

We can conclude that the calculations showed that the studied fluoroquinolone derivatives in triplet T_1 and first relevant singlet S_1 excited states are able to transfer the electron or energy to form $O_2^{\bullet-}$ or singlet $O_2(^1\Delta_g)$.

3.5. EPR experiments

Theoretical considerations on the photoinduced processes of investigated fluoroquinolones pointed to the possibility of superoxide radical anion and singlet oxygen formation upon UVA photoexcitation. Consequently, the EPR investigations were focused on the evidence of $O_2^{\bullet-}$ and $^1O_2$ for-

mation upon UVA exposure of fluoroquinolones in DMSO or ACN.

The photoinduced formation of reactive free radicals was investigated using EPR spin trapping technique, a suitable method for indirect detection of short-living radicals [91]. Table 7 summarizes the experimental EPR spectra obtained in dark after 660 s of UV exposure of fluoroquinolones DMSO solutions in the presence of DMPO along with simulations and spin Hamiltonian parameters. The UVA irradiation of all investigated fluoroquinolones in aerated DMSO in the presence of DMPO resulted in the formation of dominant twelve-line EPR signal attributed to DMPO-adduct with superoxide radical anion, •DMPO-O_2^-, characterized by spin Hamiltonian parameters a_N = 1.275 mT; a_H^β = 1.036 mT; a_H^γ = 0.139 mT and g-value = 2.0058, in good correlation with reference data [68,91,92]. The simulation analysis revealed also the presence of spin adducts originating from DMSO solvent (•DMPO-OCH_3 and •DMPO-OR [71,93,94]). In the EPR spectra of irradiated **EEFQ**, **MEFQ** and **CNFQ** also the formation of nitrogen-centered radicals trapped on DMPO (•DMPO-NR_1 and •DMPO-NR_2 [91]) was evidenced, and minor intensity of six-line signal of carbon-centered radical added to DMPO (•DMPO-CR) was found in the EPR spectra of **ACFQ**. We propose that nitrogen-centered radicals are produced *via* N1–C2 bond cleavage, in correlation with the electron distribution in the LUMO orbitals (Fig. S1). After the electron excitation from HOMO to LUMO in the hydroxy-tautomer, the electron density over the above mentioned bond is decreased.

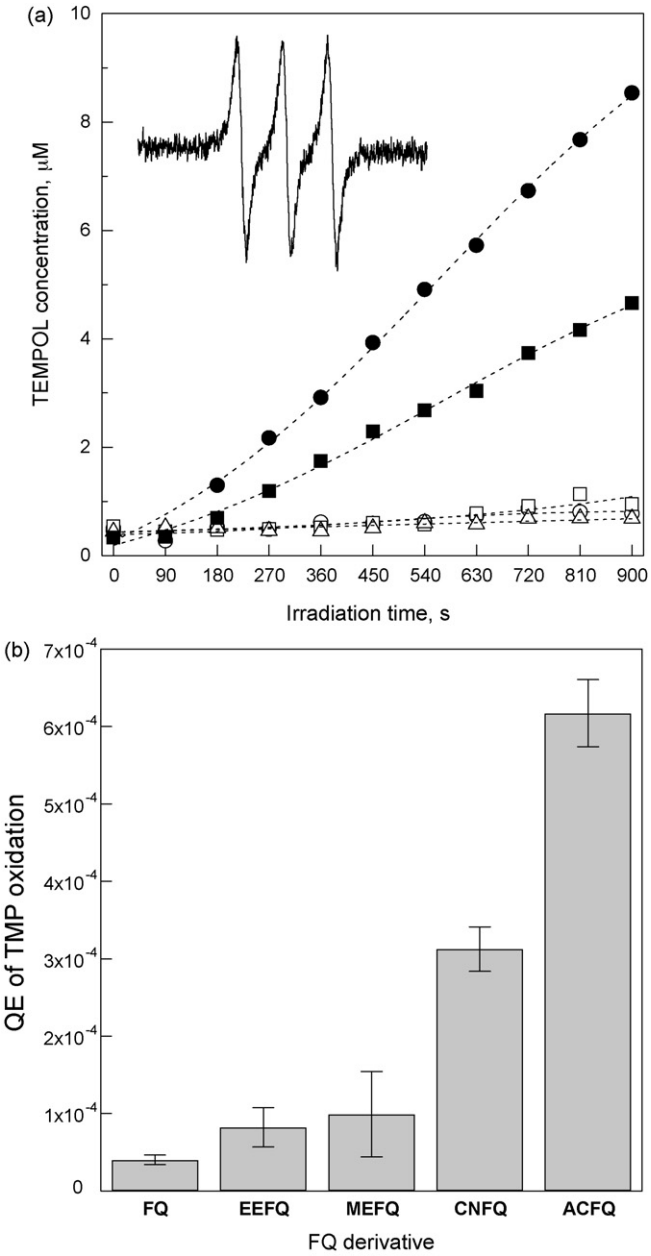

Fig. 6. (a) Time dependence of TEMPOL concentration produced *via* TMP oxidation upon irradiation of fluoroquinolone derivatives in ACN/TMP/air systems ($c_{0,TMP}$ = 0.01 M): (○) **FQ**, c_0 = 0.8 mM; (□) **EEFQ**, c_0 = 0.08 mM; (△) **MEFQ**, c_0 = 0.08 mM; (■) **CNFQ**, c_0 = 0.8 mM; (●) **ACFQ**, c_0 = 0.8 mM. Inset represents EPR spectrum of TEMPOL monitored in ACFQ/ACN/TMP/air solutions after 900 s exposure (SW = 10 mT). The symbols represent experimental data and the dotted lines were calculated by a least-squares minimization procedure using Boltzmann function. (b) Quantum efficiency (300–400 nm) of TEMPOL generated *via* TMP oxidation upon irradiation of fluoroquinolone derivatives in aerated ACN solutions.

The photoinduced generation of singlet oxygen upon continuous UVA irradiation of fluoroquinolone derivatives in ACN was evidenced *via* oxidation of TMP [68–71] to semi-stable nitroxyl radical TEMPOL characterized with three-line EPR signal (a_N = 1.575 mT; g = 2.0060; inset in Fig. 6a). The first spectrum in the time-evolution was measured without radiation, and subsequently, upon continuous irradiation ten spectra were recorded. (Each EPR spectrum represented an accumulation of two scans measured with a 45 s sweep time). The relative integral intensities of EPR signal were calculated by double-integration of the individual experimental spectra, and the concentration of photogenerated TEMPOL upon UVA exposure was determined. The obtained dependencies of TEMPOL concentration upon irradiation time shown in Fig. 6a were fitted by a non-linear least-squares method to Boltzmann function, and the initial rate of photoinduced TEMPOL formation ($R_{in,TEMPOL}$) was evaluated for individual fluoroquinolone derivatives (Fig. 6a). Generation of $^1O_2$ upon irradiation of fluoroquinolones under given experimental conditions was confirmed by the addition of sodium azide [71] into the reaction system, which caused substantial decrease of EPR signal intensity of photogenerated TEMPOL.

In order to compare the ability to act as a photosensitizer for studied fluoroquinolone derivatives, the quantum efficiency (QE; 300–400 nm, i.e. 4.13–3.10 eV) of TEMPOL generated *via* singlet oxygen oxidation of TMP was calculated [89] and the results are summarized in Fig. 6b. The presence of cyano or acetyl groups at C3 of the 4-oxoquinoline skeleton in **CNFQ** and **ACFQ** derivatives caused significant increase of TEMPOL quantum efficiency. The comparison of experimental QE and the evaluated energetic parameters of fluoroquinolones showed the linear correlation (R = −0.984) between the QE and TD-DFT lowest triplet excitation energies, $E(T_1)$, considering hydroxy-tautomer in ACN solvent (Table 2). This indicates that the vertically excited hydroxy-tautomer may play substantial role in the process of singlet oxygen generation *via* exchange electronic energy transfer.

4. Conclusions

Theoretical calculations showed that the five studied fluoroquinolone derivatives can be found in two forms – oxo- and hydroxy-tautomer. In the gas phase, the hydroxy-tautomer is preferred, while the solvents ACN and DMSO stabilize the oxo-tautomer. Presence of electron-withdrawing substituents at C3 atom of the pristine fluoroquinolone molecule affects the bonding situation and leads to a blueshift of the experimental UV/vis absorption maxima as well as of the calculated vertical excitations. Experimental UV/vis absorption spectrum in DIOX showed that the solvent is able to change the concentration ratio between oxo- and hydroxy-tautomers present in the solution.

DFT calculations indicate that in solution-phase, direct and indirect electron transfer from the studied molecules resulting

in superoxide radical anion $O_2^{\bullet-}$ can occur. These processes are thermodynamically favored. Besides, this study showed that the fluoroquinolones in excited singlet or triplet states are capable to transfer energy to molecular oxygen. This process enables formation of singlet oxygen ($^1\Delta_g$). EPR spin trapping experiments performed in DMSO using DMPO as the spin trapping agent, confirmed the photoinduced $O_2^{\bullet-}$ generation upon irradiation of all investigated fluoroquinolones. Singlet oxygen produced during photoexcitation of fluoroquinolone derivatives in ACN was monitored using EPR *via* oxidation of TMP to nitroxyl radical TEMPOL. The evaluated quantum efficiency (300–400 nm) of this process revealed significant dependence on substituent at C3 atom of quinolone skeleton. The presence of cyano or acetyl groups in this position caused the increase in the ability of the investigated fluoroquinolone derivatives to act as a photosensitizer.

Acknowledgements

This study was financially supported by Scientific Grant Agency (VEGA Projects 1/0137/09, 1/0225/08 and 1/0018/09) and Research and Development Agency of the Slovak Republic (contracts Nos. APVV-0055-07, LPP 0230-09, SK-AT-0002-08 and SK-AT-0016-08) and by the Austrian Academic Exchange Service program Wissenschaftlich-Technische Zusammenarbeit Austria-Slovakia under contract No. ÖAD WTZ 11/2009.

Appendix A. Supplementary data

Supplementary data associated with this article can be found, in the online version, at doi:10.1016/j.jphotochem.2010.02.001.

References

[1] L. Shen, W. Kohlbrenner, D. Weigl, J. Baranowski, Mechanism of quinolone inhibition of DNA gyrase—appearance of unique norfloxacin binding-sites in enzyme–DNA complexes, J. Biol. Chem. 264 (1989) 2973–2978.
[2] M. Andersson, A. MacGowan, Development of the quinolones, J. Antimicrob. Chemother. 51 (2003) 1–11.
[3] D. Hooper, J. Wolfson, Mode of action of the quinolone antimicrobial agents—review of recent information, Rev. Infect. Dis. 11 (1989) S902–S911.
[4] C. Spooner, A. Pickard, D. Menon, Drug utilization reviews of oral quinolone, cephalosporin, and macrolide use in nonacute care: a systematic review, Clin. Ther. 21 (1999) 1951–1972.
[5] R. Stahlmann, Clinical toxicological aspects of fluoroquinolones, Toxicol. Lett. 127 (2002) 269–277.
[6] M. Heller, FDA alert of quinolones and phototoxicity, J. Drugs Dermatol. 7 (2008) 501–1501.
[7] R. Mang, H. Stege, J. Krutmann, Mechanisms of phototoxic and photoallergic reactions, in: P.J. Frosch, T. Menné, J.-P. Lepoittevin (Eds.), Contact Dermatitis, Springer, Berlin, 2006, pp. 97–104.
[8] K. Stein, N. Scheinfeld, Drug-induced photoallergic and phototoxic reactions, Expert Opin. Drug Saf. 6 (2007) 431–443.
[9] N. Neumann, A. Blotz, G. Wasinska-Kempka, M. Rosenbruch, P. Lehmann, H. Ahr, H. Vohr, Evaluation of phototoxic and photoallergic potentials of 13 compounds by different in vitro and in vivo methods, J. Photochem. Photobiol. B: Biol. 79 (2005) 25–34.
[10] E. Fasani, S. Monti, I. Manet, F. Tilocca, L. Pretali, M. Mella, A. Albini, Inter- and intramolecular photochemical reactions of fleroxacin, Org. Lett. 11 (2009) 1875–1878.
[11] M. Freccero, E. Fasani, M. Mella, I. Manet, S. Monti, A. Albini, Modeling the photochemistry of the reference phototoxic drug lomefloxacin by steady-state and time-resolved experiments, and DFT and post-HF calculations, Chem. Eur. J. 14 (2008) 653–663.
[12] N. Hayashi, Y. Nakata, A. Yazaki, New findings on the structure-phototoxicity relationship and photostability of fluoroquinolones with various substituents at position 1, Antimicrob. Agents Chemother. 48 (2004) 799–803.
[13] A. Albini, S. Monti, Photophysics and photochemistry of fluoroquinolones, Chem. Soc. Rev. 32 (2003) 238–250.
[14] E. Fasani, A. Profumo, A. Albini, Structure and medium-dependent photodecomposition of fluoroquinolone antibiotics, Photochem. Photobiol. 68 (1998) 666–674.
[15] E. Fasani, M. Rampi, A. Albini, Photochemistry of some fluoroquinolones: effect of pH and chloride ion, J. Chem. Soc., Perkin Trans. 2 (1999) 1901–1907.
[16] E. Fasani, F. Negra, M. Mella, S. Monti, A. Albini, Photoinduced C–F bond cleavage in some fluorinated 7-amino-4-quinolone-3-carboxylic acids, J. Org. Chem. 64 (1999) 5388–5395.
[17] L. Martinez, R. Sik, C. Chignell, Fluoroquinolone antimicrobials: singlet oxygen, superoxide and phototoxicity, Photochem. Photobiol. 67 (1998) 399–403.
[18] L. Martinez, C. Chignell, Photocleavage of DNA by the fluoroquinolone antibacterials, J. Photochem. Photobiol. B: Biol. 45 (1998) 51–59.
[19] S. Monti, S. Sortino, Laser flash photolysis study of photoionization in fluoroquinolones, Photochem. Photobiol. Sci. 1 (2002) 877–881.
[20] N. Umezawa, K. Arakane, A. Ryu, S. Mashiko, M. Hirobe, T. Nagano, Participation of reactive oxygen species in phototoxicity induced by quinolone antibacterial agents, Arch. Biochem. Biophys. 342 (1997) 275–281.
[21] M. Cuquerella, F. Bosca, M. Miranda, A. Belvedere, A. Catalfo, G. de Guidi, Photochemical properties of ofloxacin involved in oxidative DNA damage: a comparison with rufloxacin, Chem. Res. Toxicol. 16 (2003) 562–570.
[22] M. Cuquerella, F. Bosca, M. Miranda, Photonucleophilic aromatic substitution of 6-fluoroquinolones in basic media: triplet quenching by hydroxide anion, J. Org. Chem. 69 (2004) 7256–7261.
[23] V. Lhiaubet-Vallet, F. Bosca, M. Miranda, Photosensitized DNA damage: the case of fluoroquinolones, Photochem. Photobiol. 85 (2009) 861–868.
[24] J. Rosen, Proposed mechanism for the photodynamic generation of 8-oxo-7,8-dihydro-2'-deoxyguanosine produced in cultured cells by exposure to lomefloxacin, Mutat. Res.: Fund. Mol. Mech. Mutagen. 381 (1997) 117–129.
[25] A. Kornhauser, W.G. Wamer, L.A. Lambert, Light-induced dermal toxicity: effects on cellular and molecular level, in: H. Zhai, H.I. Maibach, K.-P. Wilhelm (Eds.), Marzulli and Maibach's Dermatotoxicology, CRC Press, New York, 2008, pp. 629–658.
[26] S. Onoue, Y. Tsuda, Analytical studies on the prediction of photosensitive/phototoxic potential of pharmaceutical substances, Pharm. Res. 23 (2006) 156–164.
[27] T. Araki, Y. Kawai, I. Ohta, H. Kitaoka, Photochemical behavior of sitafloxacin, fluoroquinolone antibiotic, in an aqueous solution, Chem. Pharm. Bull. 50 (2002) 229–234.
[28] S. Itoh, S. Nakayama, H. Shimada, In vitro photochemical clastogenicity of quinolone antibacterial agents studied by a chromosomal aberration test with light irradiation, Mutat. Res. Gen. Toxicol. Environ. Mutagen. 517 (2002) 113–121.
[29] K. Yabe, K. Goto, T. Jindo, M. Sekiguchi, K. Furuhama, Structure-phototoxicity relationship in Balb/c mice treated with fluoroquinolone derivatives, followed by ultraviolet-A irradiation, Toxicol. Lett. 157 (2005) 203–210.
[30] E. Fasani, M. Mella, S. Monti, A. Albini, Unexpected photoreactions of some 7-amino-6-fluoroquinolones in phosphate buffer, Eur. J. Org. Chem. (2001) 391–397.
[31] S. Monti, S. Sortino, E. Fasani, A. Albini, Multifaceted photoreactivity of 6-fluoro-7-aminoquinolones from the lowest excited states in aqueous media: a study by nanosecond and picosecond spectroscopic techniques, Chem. Eur. J. 7 (2001) 2185–2196.
[32] T. Spratt, S. Schultz, D. Levy, D. Chen, G. Schluter, G. Williams, Different mechanisms for the photoinduced production of oxidative DNA damage by fluoroquinolones differing in photostability, Chem. Res. Toxicol. 12 (1999) 809–815.
[33] J. Rosen, A. Prahalad, G. Schluter, D. Chen, G. Williams, Quinolone antibiotic photodynamic production of 8-oxo-7,8-dihydro-2′-deoxyguanosine in cultured liver epithelial cells, Photochem. Photobiol. 65 (1997) 990–996.
[34] C. Martinez, A. Neumer, C. Marti, S. Nonell, A. Braun, E. Oliveros, Effect of the media on the quantum yield of singlet Oxygen ($O_2(^1\Delta_g)$) production by 9H-fluoren-9-one: solvents and solvent mixtures, Helv. Chim. Acta 86 (2003) 384–397.
[35] L. Martinez, G. Li, C. Chignell, Photogeneration of fluoride by the fluoroquinolone antimicrobial agents lomefloxacin and fleroxacin, Photochem. Photobiol. 65 (1997) 599–602.
[36] K.A.K. Musa, L.A. Eriksson, Photodegradation mechanism of the common nonsteroid anti-inflammatory drug diclofenac and its carbazole photoproducts, Phys. Chem. Chem. Phys. 11 (2009) 4601–4610.
[37] J.L. Brédas, J. Cornil, F. Meyers, D. Beljone, Electronic structure and optical response of highly conducting and semiconducting conjugated polymers and oligomers, in: T.A. Skotheim, R.L. Elsenbaumer, J.R. Reynolds (Eds.), Handbook of Conducting Polymers, Marcel Dekker, New York-Basel, 1998, pp. 1–26.
[38] C.E. Párkányi, Theoretical Organic Chemistry, Elsevier Science, Amsterdam, 1998.
[39] R.G. Parr, W. Yang, Density-Functional Theory of Atoms and Molecules in Chemistry, Springer-Verlag, New York, 1991.
[40] F. Furche, R. Ahlrichs, Adiabatic time-dependent density functional methods for excited state properties, J. Chem. Phys. 117 (2002) 7433–7447.
[41] R. Bauernschmitt, R. Ahlrichs, Treatment of electronic excitations within the adiabatic approximation of time dependent density functional theory, Chem. Phys. Lett. 256 (1996) 454–464.
[42] A. Becke, Density-functional thermochemistry. 3. The Role of exact exchange, J. Chem. Phys. 98 (1993) 5648–5652.
[43] E. Cances, B. Mennucci, New applications of integral equations methods for solvation continuum models: ionic solutions and liquid crystals, J. Math. Chem. 23 (1998) 309–326.
[44] E. Cances, B. Mennucci, J. Tomasi, A new integral equation formalism for the polarizable continuum model: Theoretical background and applications to isotropic and anisotropic dielectrics, J. Chem. Phys. 107 (1997) 3032–3041.
[45] S. Miertus, E. Scrocco, J. Tomasi, Electrostatic interaction of a solute with a continuum. A direct utilizaion of ab initio molecular potentials for the prevision of solvent effects, Chem. Phys. 55 (1981) 117–129.

[46] S. Miertus, J. Tomasi, Approximate evaluations of the electrostatic free energy and internal energy changes in solution processes, Chem. Phys. 65 (1982) 239–245.
[47] J.L. Pascual-Ahuir, E. Silla, J. Tomasi, R. Bonaccorsi, Electrostatic interaction of a solute with a continuum. Improved description of the cavity and of the surface cavity bound charge distribution, J. Comput. Chem. 8 (1987) 778–787.
[48] J. Tomasi, M. Persico, Molecular interactions in solution: an overview of methods based on continuous distributions of the solvent, Chem. Rev. 94 (1994) 2027–2094.
[49] J. Tomasi, B. Mennucci, R. Cammi, Quantum mechanical continuum solvation models, Chem. Rev. 105 (2005) 2999–3093.
[50] C.J. Cramer, D.G. Truhlar, Implicit solvation models: equilibria, structure, spectra, and dynamics, Chem. Rev. 99 (1999) 2161–2220.
[51] E.S. Böes, P.R. Livotto, H. Stassen, Solvation of monovalent anions in acetonitrile and N,N-dimethylformamide: parametrization of the IEF-PCM model, Chem. Phys. 331 (2006) 142–158.
[52] G. Petersson, M. Al-Laham, A complete basis set model chemistry. 2. Open-shell systems and the total energies of the first-row atoms, J. Chem. Phys. 94 (1991) 6081–6090.
[53] V. Rassolov, M. Ratner, J. Pople, P. Redfern, L. Curtiss, 6-31G*basis set for third-row atoms, J. Comput. Chem. 22 (2001) 976–984.
[54] M.J. Frisch, J.A. Pople, J.S. Binkley, Self-consistent molecular orbital methods 25. Supplementary functions for Gaussian basis sets, J. Chem. Phys. 80 (1984) 3265–3269.
[55] R.A. Kendall, T.H. Dunning Jr., R.J. Harrison, Electron affinities of the first-row atoms revisited. Systematic basis sets and wave functions, J. Chem. Phys. 96 (1992) 6796–6806.
[56] M. Head-Gordon, A. Dreuw, Single-reference ab initio methods for the calculation of excited states of large molecules, Chem. Rev. 105 (2005) 4009–4037.
[57] M.J.G. Peach, P. Benfield, T. Helgaker, D.J. Tozer, Excitation energies in density functional theory: an evaluation and diagnostic test, J. Chem. Phys. 128 (2008) 044118-1–044118-8.
[58] E. Fasani, A. Albini, M. Mella, M. Barberis Negra, F. Barberis Negra, Light and drugs: the photochemistry of fluoroquinolone antibiotics, Int. J. Photoenergy 1 (1999) 1–5.
[59] H.-R. Park, J.-J. Seo, C.S. Sung, S.L. Hyeong, K.-M. Bark, Fluorescence quenching of norfloxacin by divalent transition metal cations, Bull. Korean Chem. Soc. 28 (2007) 1573–1578.
[60] H.R. Park, C.H. Oh, H.C. Lee, J.K. Lee, K. Yang, K.M. Bark, Spectroscopic properties of fluoroquinolone antibiotics in water-methanol and water-acetonitrile mixed solvents, Photochem. Photobiol. 75 (2002) 237–248.
[61] C. Adamo, V. Barone, Toward reliable density functional methods without adjustable parameters: the PBE0 model, J. Chem. Phys. 110 (1999) 6158–6169.
[62] C. Adamo, V. Barone, Accurate excitation energies from time-dependent density functional theory: assessing the PBE0 model for organic free radicals, Chem. Phys. Lett. 314 (1999) 152–157.
[63] C. Hattig, P. Jorgensen, Derivation of coupled cluster excited states response functions and multiphoton transition moments between two excited states as derivatives of variational functionals, J. Chem. Phys. 109 (1998) 9219–9236.
[64] M.J. Frisch, G.W. Trucks, H.B. Schlegel, G.E. Scuseria, M.A. Robb, J.R. Cheeseman, J.A. Montgomery Jr., T. Vreven, K.N. Kudin, J.C. Burant, J.M. Millam, S.S. Iyengar, J. Tomasi, V. Barone, B. Mennucci, M. Cossi, G. Scalmani, N. Rega, G.A. Petersson, H. Nakatsuji, M. Hada, M. Ehara, K. Toyota, R. Fukuda, J. Hasegawa, M. Ishida, T. Nakajima, Y. Honda, O. Kitao, H. Nakai, M. Klene, X. Li, J.E. Knox, H.P. Hratchian, J.B. Cross, C. Adamo, J. Jaramillo, R. Gomperts, R.E. Stratmann, O. Yazyev, A.J. Austin, R. Cammi, C. Pomelli, J.W. Ochterski, P.Y. Ayala, K. Morokuma, G.A. Voth, P. Salvador, J.J. Dannenberg, V.G. Zakrzewski, S. Dapprich, A.D. Daniels, M.-C. Strain, O. Farkas, D.K. Malick, A.D. Rabuck, K. Raghavachari, J.B. Foresman, J.V. Ortiz, Q. Cui, A.G. Baboul, S. Clifford, J. Cioslowski, B.B. Stefanov, G. Liu, A. Liashenko, P. Piskorz, I. Komaromi, R.L. Martin, D.J. Fox, T. Keith, M.A. Al-Laham, C.Y. Peng, A. Nanayakkara, M. Challacombe, P.M.W. Gill, B. Johnson, W. Chen, M.W. Wong, C. Gonzalez, J.A. Pople, GAUSSIAN 03, Revision A. 1, Gaussian, Inc., Pittsburgh, PA, 2003.
[65] R. Ahlrichs, M. Bar, M. Haser, H. Horn, C. Kolmel, Electronic-structure calculations on workstation computers—the program system TURBOMOLE, Chem. Phys. Lett. 162 (1989) 165–169.
[66] TURBOMOLE V6.0, a development of University of Karlsruhe and Forschungszentrum Karlsruhe GmbH, TURBOMOLE GmbH, 2009. http://www.turbomole.com.
[67] P. Černuchová, G. Vo-Thanh, V. Milata, A. Loupy, Solvent-free synthesis of quinolone derivatives, Heterocycles 64 (2004) 177–191.
[68] S. Jantová, S. Letašiová, V. Brezová, Ľ. Čipák, J. Lábaj, Photochemical and phototoxic activity of berberine on murine fibroblast NIH-3T3 and Ehrlich ascites carcinoma cells, J. Photochem. Photobiol. B: Biol. 85 (2006) 163–176.
[69] L. Zang, F. vanKuijk, B. Misra, H. Misra, The specificity and product of quenching singlet oxygen by 2,2,6,6-tetramethylpiperidine, Biochem. Mol. Biol. Int. 37 (1995) 283–293.
[70] J. Inbaraj, M. Krishna, R. Gandhidasan, R. Murugesan, Cytotoxicity, redox cycling and photodynamic action of two naturally occurring quinones, Biochim. Biophys. Acta: Gen. Subj. 1472 (1999) 462–470.
[71] A. Rajendran, R. Gandhidasan, R. Murugesan, Photosensitisation and photoinduced DNA cleavage by four naturally occurring anthraquinones, J. Photochem. Photobiol. A: Chem. 168 (2004) 67–73.
[72] WinSIM, NIEHS, Research Triangle Park, NC USA 27709, 2002. http://www.niehs.nih.gov/research/resources/software/tools/index.cfm.
[73] A. De La Cruz, J. Elguero, P. Goya, A. Martínez, W. Pfleiderer, Tautomerism and acidity in 4-quinolone-3-carboxylic acid derivatives, Tetrahedron 48 (1992) 6135–6150.
[74] I. Ukrainets, N. Bereznyakova, A. Turov, 4-Hydroxy-2-quinolones 147. Synthesis and tautomerism of 2-methyl-9H-Furo-[2,3-b]quinolin-4-one, Chem. Heterocycl. Comp. 44 (2008) 833–837.
[75] T. Petrenko, F. Neese, ORCA ASA, Version 2.6.35, University of Bonn, Germany, 2008.
[76] T. Petrenko, F. Neese, Analysis and prediction of absorption band shapes, fluorescence band shapes, resonance Raman intensities, and excitation profiles using the time-dependent theory of electronic spectroscopy, J. Chem. Phys. 127 (2007) 164319.
[77] M. Nowak, L. Lapinski, J. Fulara, A. Les, L. Adamowicz, Matrix isolation IR spectroscopy of tautomeric systems and its theoretical interpretation. 2-Hydroxypyridine/2(1H)-pyridinone, J. Phys. Chem. 96 (1992) 1562–1569.
[78] J. Gao, L. Shao, Polarization effects on the tautomeric equilibria of 2- and 4-hydroxypyridine in aqueous and organic solution, J. Phys. Chem. 98 (1994) 13772–13779.
[79] M. Mphahlele, A. El-Nahas, Tautomeric 2-arylquinolin-4(1H)-one derivatives-spectroscopic, X-ray and quantum chemical structural studies, J. Mol. Struct. 688 (2004) 129–136.
[80] J. Wang, R. Boyd, Tautomeric equilibria of hydroxypyridines in different solvents: an ab initio study, J. Phys. Chem. 100 (1996) 16141–16146.
[81] L. Kononov, G. Veinberg, E. Liepinsh, I. Dipan, N. Sukhova, E. Lukevits, Synthesis and isomeric conversions of several 2-substituted 1,4-dihydro-4-oxo-3-quinolinecarboxylic acid derivatives, Chem. Heterocycl. Comp. 24 (1988) 765–771.
[82] J. Hirano, K. Hamase, T. Akita, K. Zaitsu, Structural and photophysical properties of novel dual fluorescent compounds, 1-aryl-substituted 6-methoxy-4-quinolones, Luminescence 23 (2008) 350–355.
[83] F. Belal, A. Al-Majed, A. Al-Obaid, Methods of analysis of 4-quinolone antibacterials, Talanta 50 (1999) 765–786.
[84] E. Klein, V. Lukeš, Z. Cibulková, J. Polovková, Study of N–H, O–H, and S–H bond dissociation enthalpies and ionization potentials of substituted anilines, phenols, and thiophenols, J. Mol. Struct. (Theochem.) 758 (2006) 149–159.
[85] J. Rimarčík, V. Lukeš, E. Klein, M. Ilčin, Study of the solvent effect on the enthalpies of homolytic and heterolytic N–H bond cleavage in *p*-phenylenediamine and tetracyano-*p*-phenylenediamine, J. Mol. Struct. (Theochem.), submitted for publication.
[86] K.P. Huber, G. Herzberg, Molecular Spectra and Molecular Structure. Part IV. Constants of Diatomic Molecules, Van Nostrand Reinhold, New York, 1979.
[87] M. Travers, D. Cowles, G. Ellison, Reinvestigation of the electron affinities of O_2 and NO, Chem. Phys. Lett. 164 (1989) 449–455.
[88] J. Llano, J. Raber, L. Eriksson, Theoretical study of phototoxic reactions of psoralens, J. Photochem. Photobiol. A: Chem. 154 (2003) 235–243.
[89] A.M. Braun, M.-T. Maurette, E. Oliveros, Technologie Photochimique, Presses Polytechniques Romandes, Lausanne, 1986.
[90] N.J. Turro, V. Ramamurthy, J.C. Scaiano, Principles of Molecular Photochemistry. An Introduction, University Science Books, Sausalito, CA, 2009.
[91] P. Pieta, A. Petr, W. Kutner, L. Dunsch, In situ ESR spectroscopic evidence of the spin-trapped superoxide radical, $O_2^{\bullet -}$, electrochemically generated in DMSO at room temperature, Electrochim. Acta 53 (2008) 3412–3415.
[92] A. Li, K. Cummings, H. Roethling, G. Buettner, C. Chignell, A spin-trapping database implemented on the IBM PC/AT, J. Magn. Reson. 79 (1988) 140–142.
[93] V. Brezová, S. Gabčová, D. Dvoranová, A. Staško, Reactive oxygen species produced upon photoexcitation of sunscreens containing titanium dioxide (an EPR study), J. Photochem. Photobiol. B: Biol. 79 (2005) 121–134.
[94] R. Herscu-Kluska, A. Masarwa, M. Saphier, H. Cohen, D. Meyerstein, Mechanism of the reaction of radicals with peroxides and dimethyl sulfoxide in aqueous solution, Chem. Eur. J. 14 (2008) 5880–5889.